Advanced Composites and Hybrid Materials (2024) 7:95
https://doi.org/10.1007/s42114-024-00908-4

RESEARCH

Multifunctional 3D-printed composites based on biopolymeric matrices and tomato plant (*Solanum lycopersicum*) waste for contextual fertilizer release and Cu(II) ions removal

Roberto Scaffaro[1,2] · **Emmanuel Fortunato Gulino**[1] · **Maria Clara Citarrella**[1]

Received: 23 November 2023 / Revised: 7 May 2024 / Accepted: 8 May 2024 / Published online: 21 May 2024

Abstract
The production of tomatoes faces significant challenges, including the high amount of waste generated during the harvest stage and copper-contaminated soil due to pesticide use. To address these issues and to promote a more sustainable agriculture, innovative biodegradable green composites for contextual controlled soil fertilization and Cu removal were produced by 3D-printing technology. These composites were made by incorporating NPK fertilizer flour and tomato plant waste particles (SLP) into three different biodegradable polymeric matrices: polylactic acid (PLA); a commercial blend of biodegradable co-polyesters (Mater-Bi®, MB) and their blend (MB/PLA, 50:50). Rheological characterization suggested the potential processability of all of the composites by FDM. Morphological analysis of printed samples confirmed the good dispersion of both filler and fertilizer, which also acted as reinforcement for MB and MB/PLA composites. SLP and NPK moduli were evaluated by powder nanoindentation and, for almost composites, the theoretical Halpin-Tsai model satisfactorily fitted the actual tensile moduli. The decrease in NPK fertilizer release rate and the increase in Cu(II) removal efficiency were achieved using whole 3D-printed composites. By selecting the appropriate matrix and incorporating SLP particles, it was possible to tune the NPK release rate and achieve copper absorption efficiency. Notably, MB samples containing SLP particles displayed the fastest release and the highest Cu(II) removal efficiency.

Keywords Hybrid composites · Bio-composites · Natural filler · Fertilize release · Cu removal · 3D printing

1 Introduction

Water, soil, and food contamination is currently one of the major global problems [1]. The use of copper-containing fertilizers, pesticides and fungicides has rapidly increased in the Mediterranean area over the years [2, 3]. Tomato cultivation is widespread worldwide due to its nutritional and economic value [4]. However, the excessive use of pesticides, including copper-based compounds, in tomato cultivations poses a significant risk to both the environment and human health [5]. Although pesticides may effectively control pests and diseases, they can cause long-term environmental damage by altering soil microbial communities and disrupting the balance of soil ecosystems [6]. Moreover, the mutagenic and carcinogenic effects of this element raise profound concerns about the environment and human health, making them one of the serious worldwide ecological threat [7, 8]. In addition to the risks posed by copper-based pesticides, tomato harvest also generates significant amounts of waste due to large unused portions of the crops. These scraps, if not properly managed, can lead to negative environmental impacts, including soil contamination and greenhouse gas emissions primarily resulting from their improper burning directly on the soil [4, 9]. Therefore, there is an urgent need to address the environmental risks associated with excessive copper use in tomato plant cultivations and the consequent management of their waste.

Among the biopolymeric matrices, polylactic acid (PLA) is one of the most commonly used [10, 11], particularly to obtain green composites [12]. Additionally, Mater-Bi® (MB)—a family of biopolymers widely used for applications that require biodegradability—has recently emerged

✉ Roberto Scaffaro
roberto.scaffaro@unipa.it

[1] Department of Engineering, University of Palermo, Viale delle Scienze, ed. 6, Palermo 90128, PA, Italy

[2] INSTM, Consortium for Materials Science and Technology, Via Giusti 9, Florence 50125, Italy

as a promising option for green composite production [13, 14]. Several organic biomasses, such as *Opuntia ficus indica* flour [15–17], *Posidonia oceanica* leaves [18, 19], and banana fibers [20, 21], have been successfully used as filler in biopolymeric matrices obtaining improvements in tensile properties and biodegradability. Recently, also *Solanum lycopersicum* (i.e., tomato plant, SLP) was added to MB aiming to produce 3D-printed samples [13]. The addition of up to 10% of SLP allowed optimal processability, with satisfactory dispersion of the filler in the matrix and improved tensile strength upon increasing the filler content.

Adding natural scraps to biopolymeric matrices reduces plastic usage, thus decreasing costs and promoting more eco-friendly processes. Moreover, it accelerates matrix biodegradability while enhancing mechanical performance [22, 23].

3D-printing and, more in detail, fused deposition modeling (FDM) attracted interest as an advantageous technique to produce green composites [24], due to its ability to create highly complex geometries while significantly reducing production time and costs [25–27]. FDM structures have been already successfully produced for different applications: aerospace and automotive [28], drug release devices [29], fertilizer release devices [30], and metal ions capture [31]. FDM's potential to create complex and customized structures with a specific composition has been the key to its success: by appropriately selecting process parameters such as infill and raster angle, the porosity of the devices can be tailored, thereby enabling control over release and removal kinetics [30]. Porosity, in fact, strongly influences particle delivery and metal ions capture [32].

This study aims to investigate the effectiveness of innovative biodegradable bio-composites for contextual controlled soil fertilization and Cu removal. The composites were fabricated using 3D-printing technology, adding NPK fertilizer flour and ground particles of tomato plant waste (SLP) to three different biodegradable polymeric matrices: polylactic acid (PLA); a commercial blend of biodegradable co-polyesters (Mater-Bi®, MB); their blend (MB/PLA, 50:50 ratio). By using more cost-effective biodegradable polymers and combining them with agricultural waste, it is possible to decrease the amount of polymer required. This strategy has the potential to reduce effectively and significantly the amount of plastic used and decrease the cost of the final device. Furthermore, the addition of natural fillers or agricultural scraps to biodegradable polymers can enhance mechanical property [33, 34] of the device and accelerate biodegradability [35]. Ultimately, the aim of this work is to develop a device capable of controlling the release rate of NPK, selected as a model fertilizer compound, and contextually removing copper ions resulting from excessive fertilization, thus promoting sustainable agriculture. To validate the accomplishment of this goal, evaluations were conducted in order to test the Cu removal and NPK release ability of the devices. The Peppas-Korsmeyer mathematical model was used in order to analyze release test data.

2 Experimental section

2.1 Materials and methods

2.1.1 Materials

In this study, Mater-Bi® EF51L (MB; density = 1.22 g/cm^3; melt flow index = 3.5 g/ 10 min), produced by Novamont SpA (Novara, Italy) and PLA 2003D (density = 1.25 g/cm^3; melt flow index = 6 g/ 10 min; 4.3% content of D-lactic acid monomer), purchased from NatureWorks® (Minnetonka, MN, USA) were used, both neat and in combination, to prepare green composites. MB and PLA were melt-mixed together using an internal mixer (Brabender, Germany; T = 160 °C, rotor speed = 64 rpm, t = 3 min) aiming to produce MB/PLA (50:50) blend. Both neat matrices and the prepared blend were vacuum-dried overnight at 60 °C before processing. *Solanum lycopersicum* plant waste (SLP) was generously provided by a local farm (Palermo, Italy). The plants were mowed after tomato harvesting. In this study, only the stems and leaves of the tomato plant were used; the roots were removed prior to the following process. The tomato plants were firstly cleaned by immersing them in water at room temperature. After cleaning, the plants were dried under sunlight for 7 days and then further oven-dried overnight at 40 °C to ensure complete drying. The whole plants were then ground. NPK fertilizer with 12% of nitrogen content, 12% of phosphorus content and 17% of potassium content, purchased from Flortis, Orvital S.p.A., was used. SLP and NPK were separately ground for 3 min and sieved (Controls, USA), selecting a mesh size under 150 µm aiming to achieve a smooth printing, taking into account the 0.4 mm diameter of the nozzle (see also Table 2). According to our previous studies [13, 30, 36, 37], this particle size was chosen to avoid nozzle clogging during the 3D printing process. Prior to processing, both SLP and NPK collected powders oven dried at 40 °C overnight to reduce polymeric matrices hydrolytic scission phenomena.

2.1.2 Preparation of MB, PLA and MB/PLA neat and composites filaments

Aiming to obtain a good dispersion of the fillers and achieve good printability, specific amounts of SLP and NPK were chosen to prepare hybrid biocomposites, not overcoming a total amount of 20 wt% of filler added. More in detail, nine different formulation were prepared. In detail, a Brabender internal mixer was used in order to melt mix 10% of SPL and (or) 10% of NPK to all the selected matrices (T = 160 °C for

MB and MB/PLA series and $T = 190$ °C for PLA series, rotor speed = 64 rpm, $t = 3$ min). The three neat matrices (MB, PLA, and MB/PLA) were also processed under identical conditions for the purpose of comparison. The obtained formulations were then extruded using a Haake Polylab, Germany single-screw extruder equipped with a cylindrical nozzle (thermal profile of 130–140–150–160 °C for MB and MB/PLA series and 160–170–180–190 °C for PLA). A conveyor belt system (6 m/min) was used to draw the output extrudate aiming to obtain filaments with a diameter of ~ 1.75 mm. The filaments were named based on the selected matrix and their filler contents. Formulations of the matrices and the produced composites, together with their code names, are reported in Table 1.

2.1.3 Fabrication of 3D-printed samples

The design of printed samples was performed following the procedures already reported in our previous work [30] and briefly described in Section-1 of SI. Sharebot, Next Generation (Italy) 3D printer was used and the adopted FDM parameters are summarized in Table 2.

2.2 Characterizations

2.2.1 Morphological analysis

Morphological analysis of SLP and NPK powder cross sections surfaces (cryo-fractured) of filaments and 3D printed samples was performed through Phenom ProX (Phenom-World, The Netherlands) scanning electron microscope (SEM). For more information about the operative condition, please see Section-1 of supplementary material.

2.2.2 Rheological behaviors

The study of composite rheological behaviors can provide preliminary information about filament printability. Aiming to observe the influence of SLP particles and/or fertilize on the viscosity of the polymeric matrices and their potential impact on processability [38], rheological behaviors of the obtained filaments were analyzed, using a rotational rheometer (ARES-G2, TA Instruments, New Castle, PA, USA). The tests were conducted in frequency sweep mode in the range 0.1–100 rad/s, a constant stress of 1 Pa and using a 25-mm parallel-plate geometry. A temperature of 160 °C was used for MB an MB/PLA series while 190 °C was adopted for PLA series.

Table 1 FDM process parameters

FDM parameter	Value for MB, PLA, and MB/PLA series
Nozzle temperature	160, 190, 160 °C
Nozzle diameter	0.4 mm
Bed temperature	60, 90, 60 °C
Infill rate	100%
Infill pattern	Rectilinear
Layer thickness	0.1 mm
Extrusion width	0.4 mm
Raster angle	± 45°
Printing speed	50 mm/s
Perimeter shells	4

Table 2 Formulations of used polymeric matrices and prepared bio-composites

Sample code name	MB [wt%]	PLA [wt%]	SLP [wt%]	NPK [wt%]
MB	100	0	0	0
PLA	0	100	0	0
MB/PLA	50	50	0	0
MB-SLP	90	0	10	0
MB-NPK	90	0	0	10
MB-SLP-NPK	80	0	10	10
PLA-SLP	0	90	10	0
PLA-NPK	0	90	0	10
PLA-SLP-NPK	0	80	10	10
MB/PLA-SLP	45	45	10	0
MB/PLA-NPK	45	45	0	10
MB/PLA-SLP-NPK	40	40	10	10

2.2.3 Thermal properties

Differential scanning calorimetry (DSC) analysis was performed on the neat polymeric matrices using a Chip-DSC 10 (Linseis Messgeraete GmbH, Selb, Germany). The samples were heated to 200 °C at a heating rate of 20 °C/min. Nitrogen was used as a shielding gas to avoid polymer degradation. Trace analysis was carried out using Linseis and GraphPad Prism 9 software.

2.2.4 Nanoindentation of powder

The elastic modulus of SLP and NPK particles were tested using an Anton Paar NHT^2 nanoindenter (CSM Instruments, Switzerland) equipped with a Berkovich diamond indenter, following Baraldi et al.'s method [39]. In brief, SLP and NPK particles suitable for the test were selected using an optical microscopy (Leica MS5 stereo microscope, Wetzlar, Germany) and glued on a dedicated square glass slide. The indentation experiments were performed using the following protocol: a loading ramp of 30 s, a 30 s dwell period at maximum load (15.00 mN), and a final unloading step lasting 30 s. Measures were repeated at least six times, the average values and the standard deviations were calculated.

2.2.5 Density measurements

Density measurements of powders and polymeric matrices were carried out by using a Thermo Pycnomatic Helium Pycnometer (Pycnomatic ATC, Thermofisher, USA). The measurements were performed at 25 °C, using pure Helium. Measures were repeated at least six times, the average values and the standard deviations were calculated.

2.2.6 Mechanical characterization and modeling

Tensile properties of the 3D printed samples were investigated using an Instron 3365 machine (Norwood, MA, USA), following the same method already reported in our previous work [30]. For more information about the operative condition please see Section-1 of supplementary material.

Data obtained underwent statistical analysis with an unpaired Student t-test using GraphPad Prism 9. Statistical significance was attributed to differences between datasets when the p-value obtained was lower than 0.05.

Tensile test results were compared with the outcomes predicted by the Halpin-Tsai model. In a ternary composite, the Halpin-Tsai equation can be rewritten according to Eq. (1) [40]:

$$E_{C,HT} = \frac{3}{8}E_L + \frac{5}{8}E_T \tag{1}$$

For more information about model implementation please see Section-1 of supplementary material.

2.2.7 Release of NPK fertilizer and modeling

The material's ability to release NPK fertilizer was investigated performing conductively measurement following the protocol already reported in our previous work [30]. The Peppas-Korsmeyer model was used in order to fitted the release data. For more information about release test and the modeling of the obtained data, please see Section-1 of supplementary material.

2.3 Evaluation of Cu(II) adsorption

$CuSO_4{\cdot}5H_2O$ (Merck, 99.0%) was used to prepare the Cu(II) ion solutions. The metal ion adsorption capability was assessed by immersing the 3D-printed devices in 50 mL of copper sulfate aqueous solutions (1000 mg/L) at a room temperature for 30 days. The metal concentration in the collected aliquots was assessed by using UV/vis spectrophotometer (model UVPC 2401, Shimadzu Italia s.r.l., Milan, Italy). Previously, a series of aqueous solutions containing a known amount of $CuSO_4$ were analyzed in order to obtain a calibration line. The maximum absorbance band of $CuSO_4$ water solution was detected at 810 nm. The removal efficiency (%) of the samples was calculated according to Eq. (2) [41]:

$$\text{Removal efficiency} = \text{RE}(\%) = \frac{C_i - C_f}{C_i} \times 100 \tag{2}$$

where C_i (mg/L) and C_f (mg/L) are the concentration of copper sulfate before and after adsorption tests. All the experiments were carried out in triplicate.

The surface composition of 3D-printed samples with adsorbed Cu(II) ions was collected and analyzed by energy dispersive X-ray (EDX) analysis by using an EDX probe during SEM imaging to detect the presence of Cu(II).

3 Result and discussion

3.1 Morphology of SPL and NPK powders

After the drying process, small pieces of tomato plant stems were examined using SEM to evaluate their internal morphological structure. SEM images (Fig. 1a and b) revealed that the tomato plants used in this work are characterized by circular and square-shaped voids regularly distributed along the entire length of the stem. These features could be particularly useful to achieve infiltration of the polymeric matrices into the filler, thereby potentially obtaining a mechanical reinforcing effect with the formation of an interphase [42, 43]. After this preliminary characterization, the plant was then ground into fine particles and the obtained powder was sieved, selecting the fraction under 150 µm. Relevant SEM micrographs of SLP powder are shown in Fig. 1c and d. SLP flour is characterized by an hybrid morphology: some particles showed a fibrous shape (yellow arrows), while others had a flakes-like geometry (red arrows) due to the fact that whole tomato plant was ground as received without separating the different parts: the fibrous-shaped particles likely belong to the stems, while the flakes-like ones belong to the leaves. Moreover, fibrous-shaped particles are characterized by lengths greater than 150 µm but with high aspect ratio. This feature allows them to pass through the sieve when aligned perpendicularly to the mesh. SEM images in Fig. 1d and e (close-up view and arrow) revealed that the porous structure of the stem was partially preserved even after grinding, and that some skein-shaped particles (green circle) were also sporadically present.

Relevant micrographs of ground NPK fertilizer particles are shown in Fig. 1f and g. Although they displayed some inhomogeneity in shape and size, they all exhibited a rounded geometric shape. Furthermore, NPK and SLP particles have distinct morphologies.

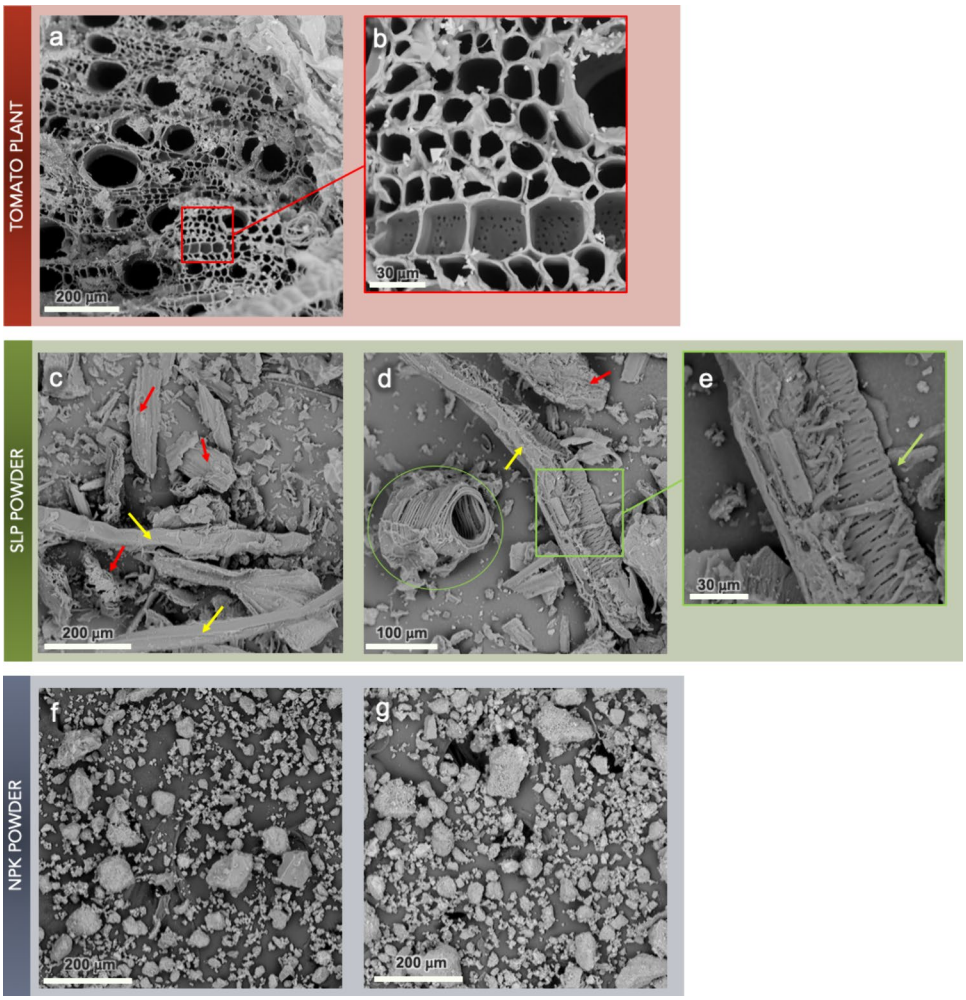

Fig. 1 SEM micrographs of tomato plant steam (**a**) and close-up view (**b**); SLP powder (**c**, **d**) and close-up view (**e**) and NPK powder (**f**, **g**). Highlighted areas in **b** and **e** provide a detailed examination of the material's microstructure

3.2 Processing and morphological analysis of filaments

First, all the different formulations (included neat MB and PLA) were melt-mixed for 2 min ($T = 160$ °C for MB and MB/PLA series and $T = 190$ °C for PLA series). The obtained mixtures were ground into pellets and then extruded into filaments using a cylindrical nozzle and a conveyor belt system. Melt mixing was performed aiming to improve the dispersion of the fillers in the polymeric matrices. This preliminary mixing enables the production of composite filaments with a homogeneous dispersion of the filler and a rounded shape, improving properties and printing performance of them. Both neat matrices and SLP and/or NPK-containing filament (diameter: ~ 1.75 mm) were successfully extruded, their morphology was analyzed, and relative optical images and SEM micrograph of their cryofractured cross section are reported in Fig. 2.

SEM micrographs confirm that all the filament showed a diameter of ~ 1.75 mm and an almost regular cylindrical shape (Fig. 2a–c; e–g; i–k) but -SLP-NPK ones that exhibited

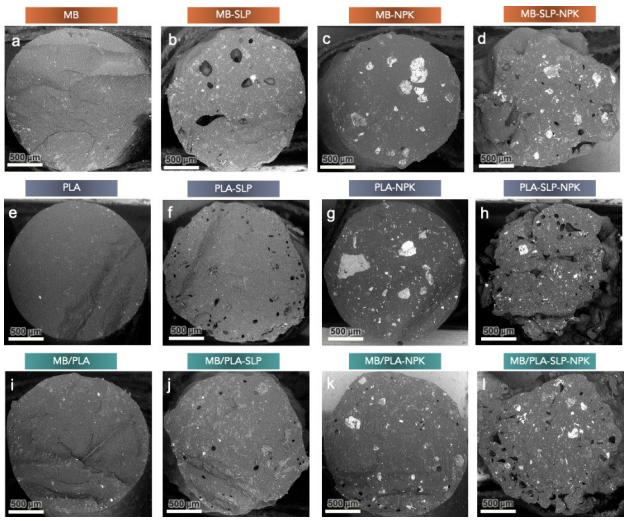

Fig. 2 SEM micrograph of MB (**a**); MB-SLP (**b**); MB-NPK (**c**); MB-SLP-NPK (**d**); PLA (**e**); PLA-SLP (**f**); PLA-NPK (**g**); PLA-SLP-NPK (**h**); MB/PLA (**i**); MB/PLA-SLP (**j**); MB/PLA-NPK (**k**); MB/PLA-SLP-NPK (**l**) filaments cross section

a non-totally uniform and quite rough surface (Fig. 2d, h, l). More in detail, MB (Fig. 2a), PLA (Fig. 2e) and MB/PLA (Fig. 2) neat filaments showed a very regular cylindrical shape. Furthermore, when blend together, MB and PLA, form an apparently homogeneous structure, at least at this scale, as shown in Fig. 2i. When just SLP is added to the different polymeric matrices (Fig. 2b, f, and j), the regular cylindrical shape and homogeneous dispersion of filler are almost preserved. SLP exhibited a good adhesion with the matrices and limited presence of voids can be noted in all three filament samples. On the other hand, the addition of NPK (Fig. 2c, g, and k) had no adverse effect on the geometric regularity of the filament. Moreover, in all filament samples, an almost homogeneous dispersion of the fertilizer with very limited presence of voids could be noted and the interfacial adhesion between the particles and the polymeric matrices seems to be good. MB-SLP-NPK (Fig. 2d), PLA-SLP-NPK (Fig. 2h) and MB/PLA-SLP-NPK (Fig. 2l) exhibit uneven edges with some voids along them. This can be explained taking into account that in this latter case the total amount of fillers (i.e., SLP and NPK) is 20%, and no more 10%. However, the cylindrical shape is sufficiently preserved in order to be 3D printed, and both the filler and the fertilizer are homogeneously dispersed throughout the filaments. The neat matrices and the SLP and(or) NPK-containing formulations showed morphology potentially suitable for FDM printing process.

3.3 Rheological behaviors and thermal properties of filaments

Filaments printability by FDM technology is strongly related to their rheological behavior [44]. Therefore, rheological analyses were investigated by using rotational rheometer and results are reported in Fig. 3a–c.

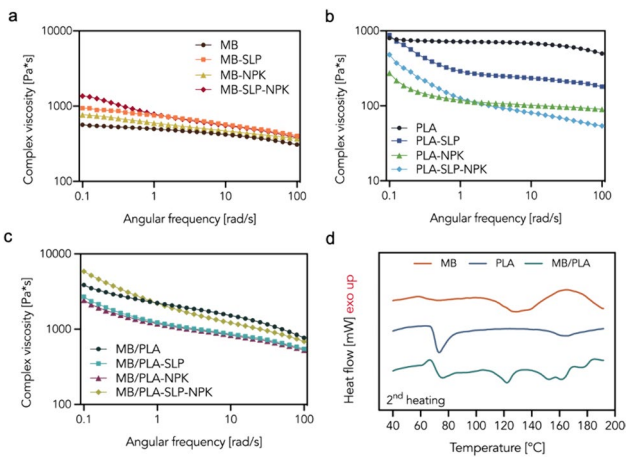

Fig. 3 Complex viscosities of MB (**a**), PLA (**b**), and MB/PLA (**c**) series performed at 160 °C, 190 °C, and 160 °C, respectively, and DSC curves (d) of the polymeric matrices

Based on our previous works [15, 38], all the formulations based on MB, PLA, and MB/PLA displayed viscosity values that are potentially suitable for be 3D-printed. More in detail, MB (Fig. 3a) shows an almost Newtonian behavior at lower frequencies and a shear-thinning behavior at higher ones. The presence of SLP or NPK lead to an increase in viscosity values across the whole range of frequency, and a more pronounced non-Newtonian behavior. When compared to MB-NPK, MB-SLP displayed higher viscosity value, possibly due to the porous and spongy structure of SLP particles that allows the polymeric matrix to infiltrate it. This tendency further increases when both SLP and NPK were present in the composite and the onset of yield stress phenomena could be observed. In this latter case, it is necessary to consider that the total amount of the dispersed phase was 20% (10% SLP nd 10% NPK)and no more 10% (SLP or NPK only) like in the previous analyzed systems. On the other hand, neat PLA (Fig. 3b) displayed its typical [45, 46] Newtonian behavior at lower frequencies and a slight shear-thinning in the higher ones region. The addition of SLP or NPK into the PLA matrix significantly lowered the complex viscosity over the entire investigated frequencies range (0.1–100 rad/s), as already reported for similar composite systems [44], suggesting a decrease of the molecular weight (M_w) due to a deterioration of the polymer phase upon processing. In the PLA composite filament (Fig. 3b), a slight change in the shape of the curve was observed: PLA-SLP, PLA-NPK, and PLA-SLP-NPK exhibited a non-Newtonian behavior at lower angular frequencies and pronounced shear-thinning behavior at higher frequencies. Moreover, for PLA-SLP-NPK the presence of yield stress phenomena could be observed. The presence of yield stress, in fact, is typical of composite systems. In Fig. 3c, the complex viscosities of the MB/PLA series are reported. The rheological behavior of MB/PLA blend was mostly influenced by the PLA phase. In the case of MB/PLA series, in fact, it should be considered that the temperature of 160 °C (used for filament preparation and sample printing), was chosen in order to limit MB thermal degradation. Therefore, at this temperature, the PLA phase was not completely molten. Due to the presence of this partially molten phase, neat MB/PLA exhibited a non-Newtonian behavior characterized by a shear-thinning behavior at high angular frequencies and the onset of yield stress phenomena at lower frequencies. The presence of SLP or NPK leads to a decrease in viscosity values across the entire frequency range, but almost no change in the shape of the curve was observed. When both SLP and NPK were present in the composite (MB/PLA-SLP-NPK), a more pronounced non-Newtonian behavior and yield stress phenomenon could be noted.

The results suggest that the rheological behaviors of all the composite filaments were compatible with the 3D printing process, especially those of the MB/PLA series. Shear-thinning properties are fundamental for lowering viscosity values, aiming to improve filament printability for 3D printing.

In order to deeply investigate the behavior of the blend, DSC measurements were performed on the neat matrices and the obtained results are presented in the form of thermogram plots in Fig. 3d. MB and PLA exhibited the same glass transition temperature of about 75 °C and melting point of 130 °C and 165 °C, respectively. MB/PLA showed almost the same glass transition temperature of the single polymeric component (about 75 °C) and two different melting points: the first at about 125 °C followed by a second at about 160 °C likely related to the melting of the PLA phase. Considering that MB is a blend of aromatic and aliphatic biodegradable co-polyesters reasonably including PLA [14], the total melting enthalpy of the different matrices could be compared in order to obtain information about the crystallinity of the materials. The thermal properties of PLA confirm a typical almost amorphous behavior of PLA, while MB exhibited a much higher melting enthalpy value showing similar results to other research studies [14]. When MB and PLA are mixed together, a higher melting enthalpy is observed reasonably due to the occurrence of a nucleation effect as already reported for similar systems [47].

3.4 3D printing and morphological analysis of composites

MB, PLA, and MB/PLA composites filament with 10% of SLP and/or NPK powders were successfully extruded obtaining a diameter of about 1.75 mm. Pure MB, PLA, and MB/PLA filaments were also produced using identical procedure for comparison. All filaments were easily 3D printed for FDM as was predicted considering SEM analysis (Fig. 2) and their rheological behaviors (Fig. 3a–c). The FDM process, in fact, proceeded smoothly, without any interruption, (also for -SLP-NPK ones despite the non-uniform surface of the filaments) and no nozzle clogging occurred. All the composites formulations could be actually printed without varying the temperature normally used for MB and PLA pure matrices (160 °C and 190 °C, respectively). Neat MB/PLA and its composites have been fluidly printed at 160 °C. Specimens of $60 \times 10 \times 1$ mm have been successfully printed with all the prepared formulations (Fig. S1).

Morphological characterization was conducted on the cryofractured cross section of 3D printed composite samples, see SEM micrographs in Fig. 4.

A relatively uniform dispersion of both natural filler and fertilizer was observed in all the composites (Fig. 4a–i). In MB (Fig. 4a–c) and PLA-based composites (Fig. 4d–f), imperfect adhesion was observed between the matrices and both SLP and NPK particles, as noted by the presence of many voids in the fracture surface. This behavior was more pronounced with SLP particles. On the other hand, both SLP and NPK particles appeared to be well-embedded in the MB/PLA matrix (Fig. 4g-i) and the adhesion between matrices and particles seemed to be good, especially for SLP particles (see red circle and arrow in Fig. 4g and i, respectively). In this latter case, the matrix penetrated inside the SLP particle pores, anchoring the particles to the matrix and achieving excellent adhesion. Moreover, all FDM-printed samples exhibited a porous structure created by the separation points among adjacent raster layers due to the selected raster angle ($\pm 45°$). The production of porous devices is really interesting because it allows water transport across the samples, enhancing fertilizer release and pollutant removal [48, 49].

3.5 Nanoindentation of SLP and NPK powders

Elastic modulus (E) of SLP and NPK particles have been investigated using nanoindentation. The nanoindentation test showed that the elastic modulus of NPK fertilizer is significantly higher than that of SLP. Specifically, Young's modulus of NPK was found to be 12,708($\pm$8.7) MPa, while SLP one was 171($\pm$0.1) MPa. This difference in stiffness between NPK and SLP can be attributed to the material's nature: NPK, in fact, is composed of a mixture of nitrogen, phosphorus, and potassium salts, which are known for their hardness and strength. On the other hand, SLP is made up of organic compounds, which tend to be relatively soft.

3.6 Mechanical properties of 3D printed composites and Halpin-Tsai model

The mechanical performance of 3D-printed composite samples was investigated through tensile tests and the outcomes of composite elastic modulus, normalized to those of each matrix, are shown in Fig. 5. The values of elastic modulus (E), tensile strength (TS), and elongation at break (EB) are reported in Table S2. The addition of SLP particles to MB (Fig. 5a, first group of bars) did not lead to any statistically relevant variation in the *E* value (see Fig. S2). To address this behavior, the fractured cross-section of MB-SLP was analyzed by SEM. As shown in Fig. 5b, during the fracture phase, SLP particles were pulled out of the polymeric matrix limiting their reinforcing effect. On the other hand, the addition of NPK to MB (MB-NPK and MB-SLP-NPK) led to a slight but statistically significant (see Fig. S2) increase in E, going from 89 MPa of neat MB to 94 and 95 MPa of MB-NPK and MB-SLP-NPK respectively.

Regarding the PLA series (Fig. 5a, second group of bars), the addition of SLP or NPK particles, or both contextually, to PLA led to a slight but statistically significant (see Fig. S2)

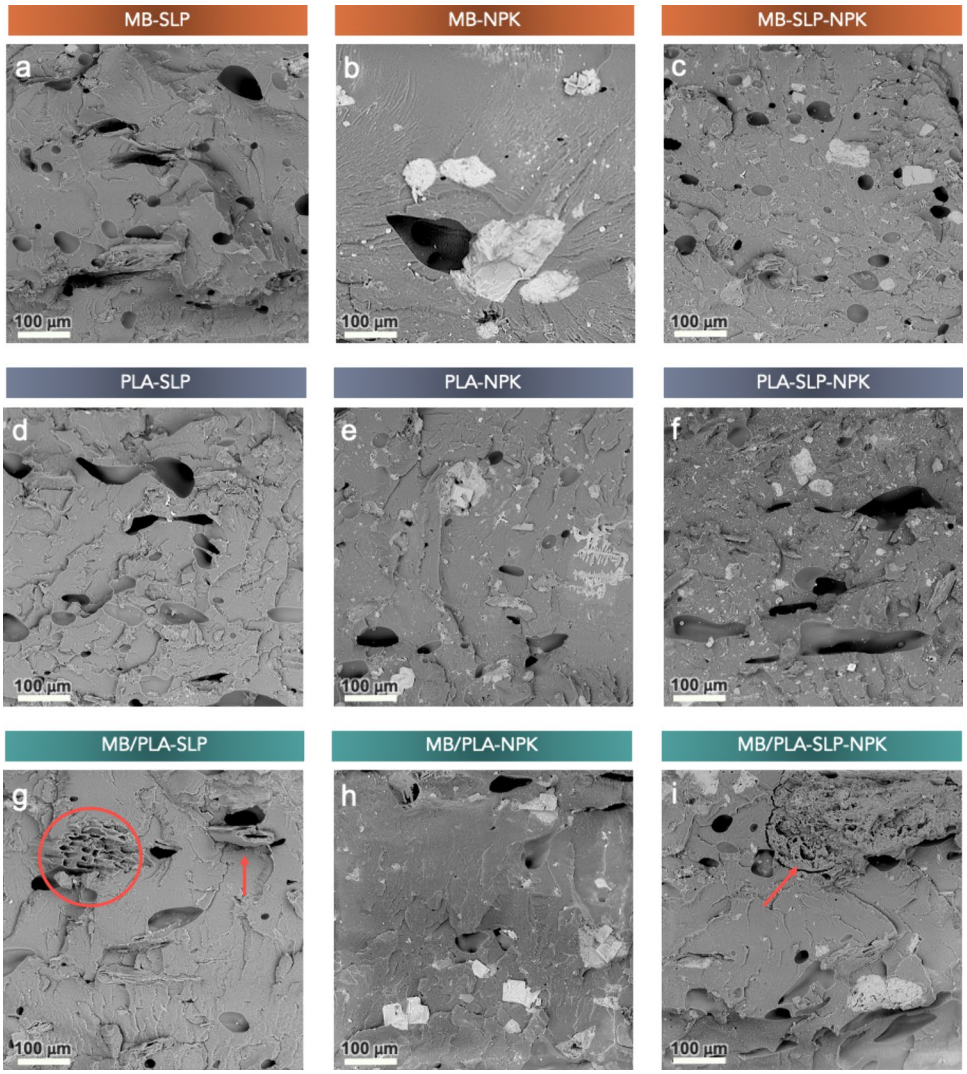

Fig. 4 SEM micrograph of MB-SLP (**a**); MB-NPK (**b**); MB-SLP-NPK (**c**); PLA-SLP (**d**); PLA-NPK (**e**); PLA-SLP-NPK (**f**); MB/PLA-SLP (**g**); MB/PLA-NPK (**h**); and MB/PLA-SLP-NPK (**i**) cross section of 3D printed samples

decrease in *E*, going from 891 MPa of neat PLA to 852, 820 and 850 MPa of PLA-SLP, PLA-NPK, and PLA-SLP-NPK, respectively. These results appear to be in full agreement with those obtained during rheological characterization. MB/PLA blend showed a different mechanical behavior (Fig. 5a, third group of bars). The addition of SLP particles led to an increase in *E*, going from 503 MPa of neat MB/PLA to 635 MPa of MB-SLP. In fact, the filler is currently well-integrated into the polymeric matrix, acting as a reinforcement (see SEM images in Fig. 4). This is evident from the observed fracture behavior during tensile testing (Fig. 5c), where SLP particles tend to break rather than pull out from the matrix. These results suggest that the filler-matrix interface is strong, allowing efficient load transfer and improved mechanical properties of the composite, in accordance with the morphological analysis, (Fig. 4h). The same trend was also observed when NPK is added to the matrix, reaching a Young's modulus of 674 MPa. Similarly, the hybrid composite (MB/PLA-SLP-NPK) exhibited the highest increase in Young's modulus, exhibiting an *E* value of 707 MPa due to the fact that the total amount of particles (SLP and NPK) is 20%. For MB/PLA series, all variations were statistically significant (see Fig. S2) and the tensile behaviors seems to be mainly influenced by the reinforcing effect given by the fillers that stiffen the composites reducing their flexural deformability (see Table S1).

Nevertheless, it should be considered that the tensile properties of these types of systems can be optimized if a raster angle of 0° is chosen. In fact, in a previous work [13], we prepared green composites based on MB and tomato plant, and we printed them with a 0° or ±45° raster angle in order to evaluate their influence on the tensile properties of the composites. Tensile test result reveals that the 0° raster angle definitively optimizes the tensile properties, confirming data from the literature, obtained on similar systems, where 0° raster angle usually optimizes tensile properties [34]. However, in this case, a raster angle of ±45° was chosen aiming to produce a more porous structure by creating separation points among adjacent

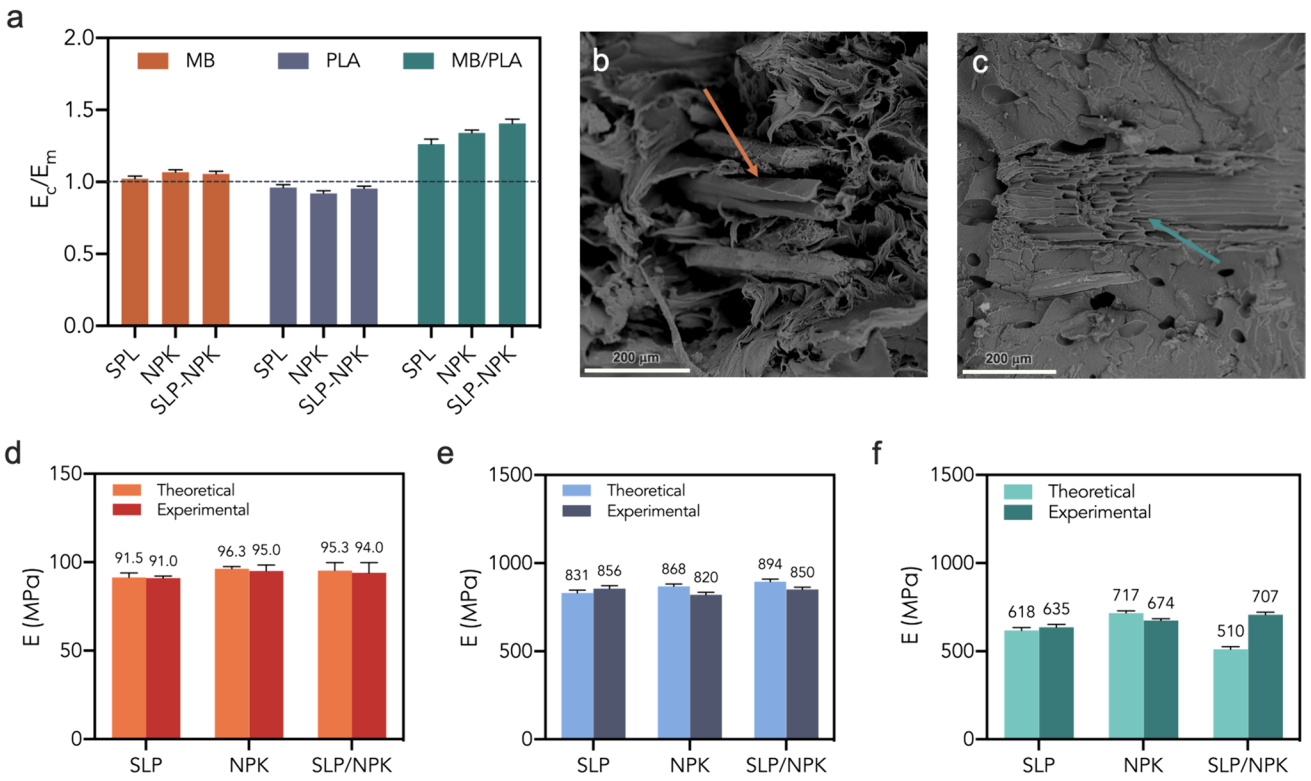

Fig. 5 Reduced elastic modulus of the composites (E_c, i.e., normalized to those of each matrix E_m), dashed line refers to neat matrices value of the reduced property (**a**); SEM micrograph of SLP particles behavior during tensile fracture in MB-SLP (**b**) and MB/PLA-SLP (**c**) printed samples; **b** theoretical and experimental elastic modulus of MB (**d**), PLA (**e**) and MB/PLA (**f**) composites

raster layers. This promotes NPK release and Cu absorption, generates channels along the devices, and allows water to be conveyed inside the sample.

The experimental data obtained in tensile tests and those predicted by Halpin–Tsai model, according to Eq. (1), were analyzed. E_{SLP} and E_{NPK} were determined by nanoindentation, as reported in the experimental part. Density measurements were performed on matrices, SLP, and NPK, and the relative results are reported in Table S2. Figure 5d–f provides a comparison between the experimentally measured tensile moduli of MB, PLA, and MB/PLA printed composites and those predicted by the Halpin-Tsai model. For MB based composites, the theoretical model satisfactorily fitted the actual tensile moduli. On the other hand, for PLA composites, the theoretical model almost fitted the tensile modulus of PLA-SLP but overestimated PLA-NPK and PLA-SLP-NPK ones. This behavior could be attributed to the imperfect adhesion between the matrix and filler and the variable aspect ratio of the fillers, especially SLP. For MB/PLA blend composites a similar behavior to that observed for PLA was noticed for MB/PLA-SLP and MB/PLA-NPK. However, for MB/PLA-SLP-NPK, the theoretical model clearly underestimated the actual tensile modulus. This issue could be addressed by considering that some SLP fibers were uniaxially oriented in tensile direction (see Fig. 6), while the used Halpin-Tsai model fitted composites reinforced with randomly oriented fibers only.

The performances of SLP-filled composites in the tensile test were strongly influenced by uniaxially oriented fibers. Moreover, the presence of SLP, NPK or both during the preparation of the MB/PLA composites blend led to the production of matrices that were slightly different from the neat one, allowing to obtain a finer dispersion of one polymeric phase in the other (see whiter sphere in Fig. S3).

3.7 NPK release and Peppas-Korsmeyer model

Conductivity measurements were used to determine the release profile of NPK from the 3D-printed samples. More in detail, electrolyte resistance was measured and correlated to the total concentration of electrolytes in solution. All tests were performed in water at 25 °C. It should be noted that this evaluation method, performed in water, may overestimate the NPK release compared to what typically occurs in soil. As a control, conductivity measurements were also performed for free NPK and for composites that do not contain NPK (see Figs. 7a and S4). When immersed in water, free NPK immediately achieved a plateau region, releasing all

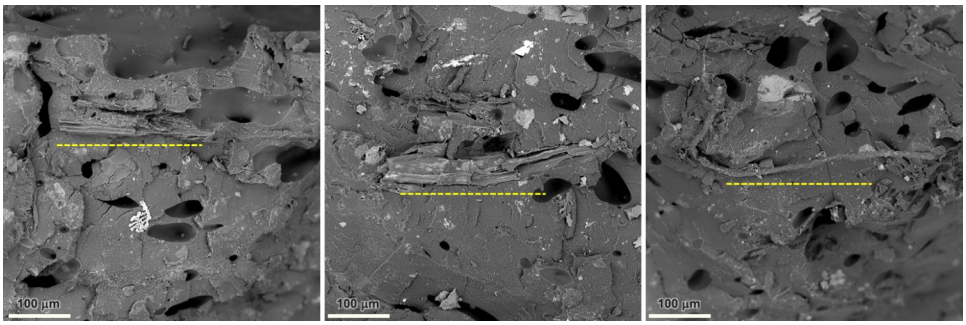

Fig. 6 SEM micrograph of MB/PLA-SLP-NPK cross section of printed samples fractured in liquid nitrogen lengthwise

fertilizer within the first 24 h. Devices without NPK (MB, MB-SLP, PLA, PLA-SLP, MB/PLA, MB/PLA-SLP) did not release any significant concentration of electrolytes after 30 days of immersion.

Conductivity tests were also conducted on NPK-filled composites to determine their release kinetics and the results are shown in Fig. 7b. The NPK release kinetics of all the 3D-printed composites were characterized by three phases: a burst release in the initial 24 h of immersion, a subsequent phase of progressive and slower release, and a final plateau region observed after 15 days of immersion, in agreement with already reported similar systems [30, 50].

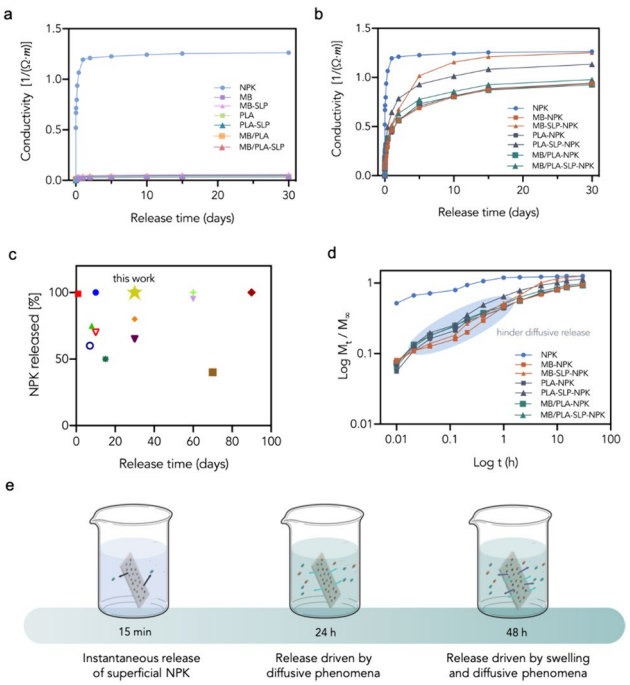

Fig. 7 Fertilizer release as function of time for free NPK, composites that not contain NPK (**a**) and 3D-printed devices (**b**); comparison of release rate of MB-SLP-NPK with other CRFs device obtained with different methods (**c**); logarithmic plots of the Peppas-Korsmeyer model power law applied to the release data collected in the burst region, $M_t/M_\infty < 0.6$ was highlighted by colored portion of the plot (**d**); pictorial description of NPK release mechanism (**e**)

The sustained release of NPK fertilizer was achieved for both composites (-NPK) and hybrid composites (SLP-NPK) prepared using the three different matrices. All composites showed a significant reduction in the amount of released NPK and therefore in conductivity values, especially in the first 24 h, compared to free NPK. Moreover, the NPK release rate could be modulated by adding SPL particles. In detail, MB-SLP-NPK showed the fastest delivery with about 80% of NPK released in the first week of the test, followed by PLA-SLP-NPK with 70% of NPK released. Other composites exhibited a lower release of NPK: after 7 days, MB/PLA-SLP-NPK released about 60% of NPK while all the composited that not contain SLP released about 55% of it. In fact, when the samples were immersed in water, SLP particles were also released into the aqueous medium, generating channels along the devices and allowing the water to be conveyed inside the sample.

This suggests that NPK particles, found within the interior of the samples, may have a higher potential to be released. Moreover, a weak adhesion between matrix and filler would promote filler and fertilize release, thus justifying the more inhibited release of MB/PLA systems. Therefore, the results imply that, if a faster and complete release is required, SLP particles should be added to the composites and MB should be preferred as polymeric matrix. MB-SLP-NPK system, in fact, release 100% of NPK after 30 day of immersion, achieving a complete release of the fertilize. The quantity of NPK released for each sample after 30 day is reported in Table S3. When compared to other controlled-release fertilizer devices mentioned in the scientific literature, the devices produced in this study displayed a remarkable capacity to reduce the release rate of NPK, as evident in Fig. 7c [51–53].

The obtained NPK release data was evaluated by plotting logarithmic graphs as a function of time (Fig. 7d) to gain a better understanding of the fertilizer release mechanism. During the firsts 24 h of release test, burst release was observed. This phase can be divided in two sub-phases: at first the fertilizer available on composites surface was rapidly delivered (within the first 15 min) and subsequently the delivery was driven by diffusive phenomena (colored portion of the plot).

As the release progressed, the release curves showed an increase in slope likely due to the occurrence of swelling phenomena across the polymeric matrix possibly caused by the higher porosity induced by the printing process that reasonably led to a relevant increase in water uptake for FDM structures [30]. In the final stage, fertilizer delivery was reasonably governed by both swelling and diffusive phenomena. Peppas-Korsmeyer mathematical model [54] was used to fit the obtained release data and confirm the hypotheses on NPK release mechanism [55]. This model has previously been successfully used to describe fertilizer release kinetics from CRFs devices [30, 56]. The values of K and n of the different formulations were determined and reported Table 3.

Analyzing the calculated n value is possible to make assumption about the release mechanism: n approximately 0.5 indicate a diffusion-driven release; when $n = 1$ swelling occurs and when n values are between 0.5 and 1 both swelling and diffusive phenomena occurs [32]. A value of $n < 0.5$ may indicate that the matrix hinders the diffusion of the particles. As seen previously, the release curves of all composites are characterized by a burst region that represent two different effect:

(i) NPK particles readily available on the device's surface are immediately delivered in the aqueous media ($t = 15$ min)
(ii) The real capability of the 3D-printed devices to perform a controlled release

In this second region, all the systems displayed n <0.5 (see n value in Table 3); therefore, the fillers could indeed slow the fertilizer release. In general, in the first 24 h, all the composites showed a hindered diffusion of the NPK, especially PLA-NPK, MB/PLA-NPK, and MB/PLA-NPK (n = 0.33, 0.32, 0.36, respectively). CRFs composites showed an almost diffusive release mechanism, unlike NPK grains. In fact, in this latter case, NPK is immediately released for erosive dissolution. Figure 7e provides a pictorial representation of the release mechanism of the CRFs composites described above.

Table 3 Values of slopes (n) and intercepts (k) of fitting of power law applied to the release data collected in the burst region ($M_t / M_\infty <$ 0.6)

Sample	K	n
MB-NPK	0.46	0.42
MB-SLP-NPK	0.41	0.43
PLA-NPK	0.48	0.33
PLA-SLP-NPK	0.59	0.41
MB/PLA-NPK	0.48	0.32
MB/PLA-SLP-NPK	0.53	0.36

Morphology of CRF devices was analyzed also after 30 days of soaking in water. Optical image (Fig. 8a-f) and SEM micrograph (Fig. 8a'–f') of the 3D-printed samples before (Fig. 8a–c and a'–c') and after (Fig. 8d-f and d'-f') NPK release were reported. Before the release, all the samples exhibited a satisfying adhesion of adjacent layer especially MB/PLA one (Fig. 8c and c') that also showed an excellent print definition. After soaking in water for 30 days, instead, PLA sample (Fig. 8e and e') showed a clear detachment of the layers, which was even more marked for MB one (Fig. 8d and d'). This behavior testifies the occurrence of swelling of the polymeric matrices confirming the supposed mechanism of release. Moreover, the PLA samples appear discolored after release, likely due to filler loss, as observed by comparing the optical images in Fig. 8b and e. With regard to the MB/PLA samples, the swelling phenomenon was less evident compared to MB and PLA ones. From the SEM micrograph in Fig. 8e', it is possible to observe that the layers do not show any detachment, but on the contrary, they appear to be better adherent to each other. Once again, this different behavior may be caused by the greater crystallinity of the blend compared to one of the single components. Moreover, this behavior reasonably explains the slower NPK release obtained for the MB/PLA samples compared to that recorded for MB and PLA ones.

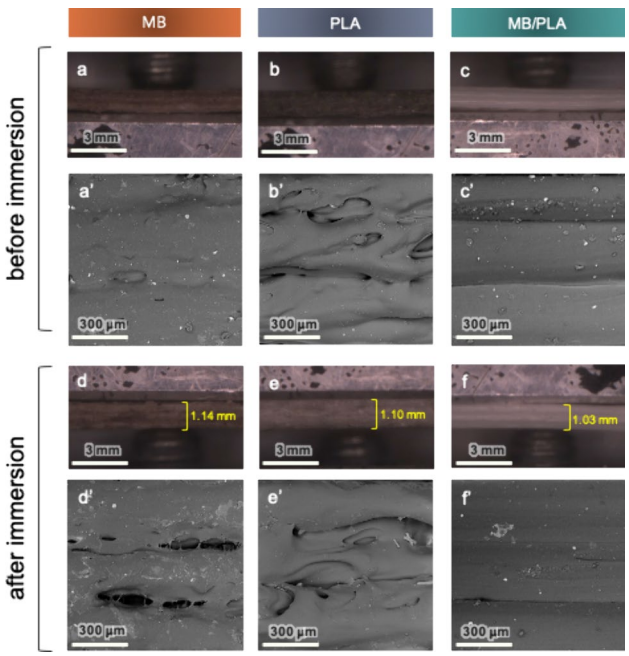

Fig. 8 Optical image (a–f) and SEM micrograph (a'–f') of good adhesion between layers in FDM samples before NPK release (a–c and a'–c') and layers detachment in FDM samples after soaking in water for 30 days due to occurrence of swelling (d–f and d'–f')

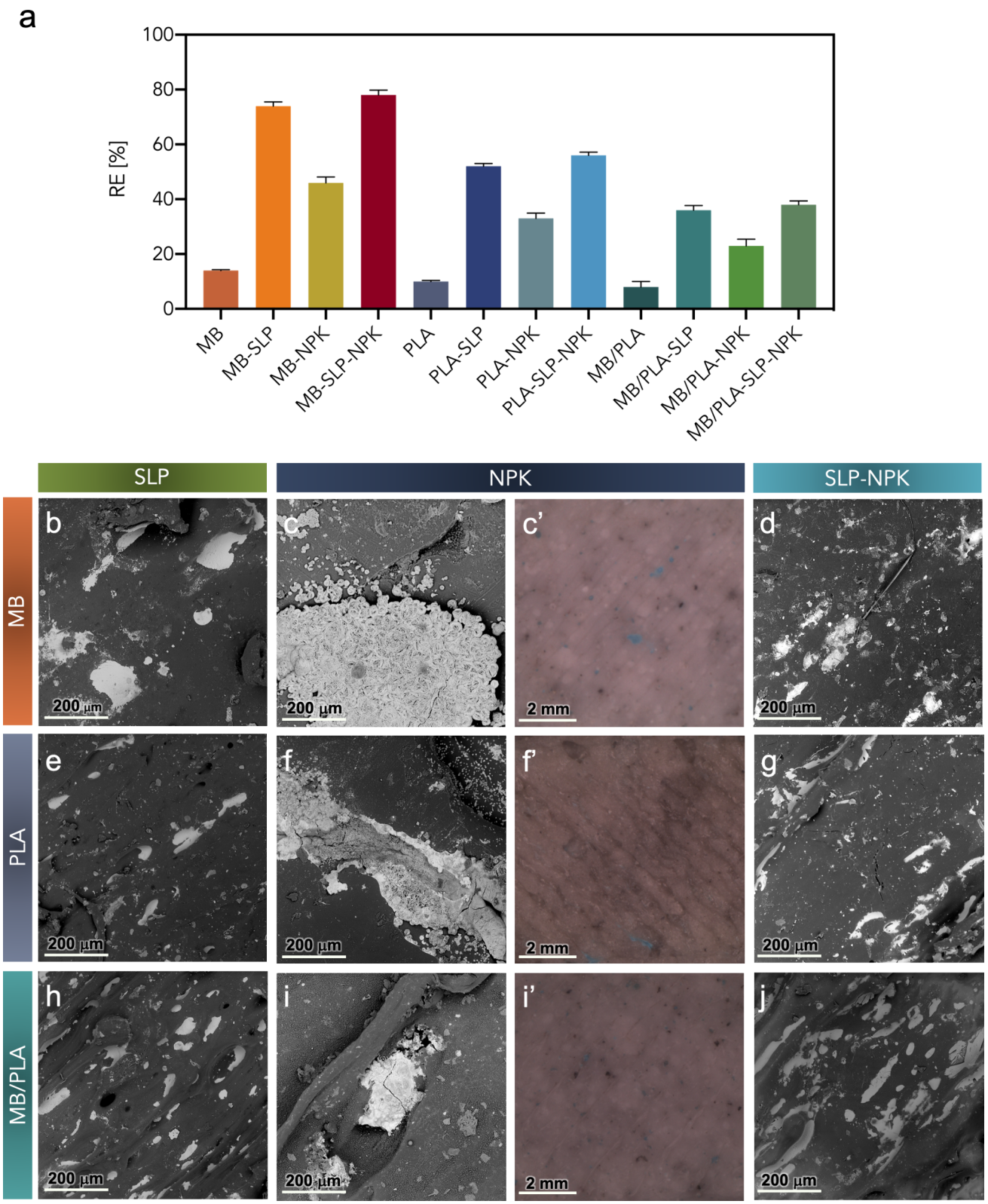

Fig. 9 Removal efficiency of the devices (**a**) and SEM micrographs (**b–j**) and optical images (**c'**, **f'**, **i'**) of the green composites after the immersion in copper sulfate aqueous solutions for 30 days

3.8 Cu(II) absorption

All the 3D-printed green composites were separately immersed in copper sulfate aqueous solutions for 30 days. UV spectroscopy was employed to test the Cu(II) ion removal efficiency of the samples, calculated according to Eq. (4), and the outcomes are reported in Fig. 9a. All the green composites exhibited a significant increment in the removal efficiency over the neat MB, PLA, and MB/PLA that were 14, 10, and 8%, respectively. Despite plastics are considered inert, previous studies have reported the adsorption of metal ions onto various biopolymeric material, including PLA and PBAT [31, 57]. The highest removal efficiency for all the three type of matrices was observed for the -SLP an -SLP-NPK composites. In detail, the maximum removal efficiency was achieved by MB-SLP-NPK with 78% of Cu removed from the aqueous solution, followed by MB-SLP with 74%. MB-NPK showed a removal efficiency of 46%. Both PLA and MB/PLA composites showed the same trend. However, in both cases, a lower removal efficiency was achieved, especially for MB/PLA composites, which exhibited the lowest values. This behavior can be explained by considering the more compact structure of the MB/PLA samples, which remains almost unchanged after immersion in water for 30 days, preventing water from being conveyed inside the sample and thus reducing the surface area available for the absorption.

These results clearly demonstrated that Cu removal efficiency of the composites could be modulated by adding SPL particles. Indeed, the composites that do not contain SLP exhibited the lowest removal efficiency values of the series. This behavior could be reasonably explained by taking into account that, SLP contains natural compounds such as cellulose, lignin, and hemicellulose that have a high affinity for metal ions [2, 58]. It is reasonable to assume that these compounds can absorb copper ions, effectively removing them from the aqueous solution. Moreover, the release of NPK particles generated channels along the polymeric matrices, facilitating the water to be conveyed inside the sample. This promoted the contact with more SLP particles, resulting in higher removal efficiency for -SLP-NPK samples. SEM images in Fig. 9b–j reveal that, for the -SLP and -SLP-NPK samples, the majority of the copper was absorbed by the SLP particles, identifiable as white spots in the micrographs (confirmed by punctual EDAX analysis; sample test identifying copper on white spots; see Fig. S5). On the other hand, for the -NPK samples (as shown in SEM and optical images in Fig. 9c–c', f–f', and i–i') Cu(II) clusters formed on the polymeric matrices (confirmed by punctual EDAX analysis; sample test identifying copper on white spots; see Fig. S5) which could also be easily identified through visual inspection thanks to the pale color of the composites.

4 Conclusions

Biodegradable green composites for contextual controlled soil fertilization and Cu removal were produced by 3D-printing. NPK fertilizer flour and tomato plant waste particles (SLP) were added to three different biodegradable polymeric matrices: polylactic acid (PLA), a commercial blend of biodegradable co-polyesters (Mater-Bi®, MB) and their blend (MB/PLA, 50:50). All the obtained filaments were successfully printed by FDM, in agreement with morphological analysis and rheological characterization. Morphological analysis performed on the cross section of 3D printed composite samples confirmed a relatively uniform dispersion of both natural filler and fertilizer in all composite samples. Moreover, MB and MB/PLA samples displayed good adhesion between the fillers and the matrix, unlike PLA ones where imperfect adhesion was observed. These behaviors affect the mechanical performance of the composites. For MB and MB/PLA the filler and the fertilize effectively act as reinforcement. SLP and NPK elastic moduli were evaluated by powder nanoindentation and, for the majority of the composites, the theoretical Halpin-Tsai model satisfactorily fitted the actual tensile moduli. NPK release tests showed the ability of all the obtained composites to slow the release rate of the fertilization up to 30 days. Moreover, it was possible to tune the release kinetics by changing the polymeric matrix and adding the natural filler (SLP). Cu(II) removal tests confirmed that all the green composites exhibited a significant increment in the removal efficiency over the neat matrices. More in detail, the Cu removal efficiency could be increased by adding SPL particles that, as expected, have been very successful in absorbing copper. MB-SLP-NPK showed 100% release of NPK after 30 days and the highest copper removal ability with 78% of Cu removed from the aqueous solution. Moreover, the addition of SLP particles leads to a decrease in the amount of polymer needed, resulting in a lower cost of the final device. In addition, the use of FDM as the selected production technique allows to reduce production time and costs. Considering the release kinetics results and Cu absorption test, it is possible to conclude that by adding tomato plant waste particles to polymeric matrices, it was possible to produce biodegradable, cost-effective, and easy-to-produce devices for contextual and efficient fertilizer release and Cu(II) ions capture.

Supplementary information The online version contains supplementary material available at https://doi.org/10.1007/s42114-024-00908-4.

Acknowledgements Nanoindentation experimental data were provided by ATeN Center of University of Palermo.

Author contribution Maria Clara Citarrella: writings—original draft; Roberto Scaffaro and Maria Clara Citarrella: writing—review and editing; Emmanuel Fortunato Gulino and Maria Clara Citarrella: software, formal

analysis, investigation, visualization; Roberto Scaffaro, Emmanuel Fortunato Gulino and Maria Clara Citarrella: conceptualization, data curation, methodology, validation; Roberto Scaffaro: supervision, resources, project administration, funding acquisition.

Funding Open access funding provided by Università degli Studi di Palermo within the CRUI-CARE Agreement. SAMOTHRACE (Sicilian micro and nano technology research and innovation center) extended partnership and received funding from the European Union Next-GenerationEU (PIANO NAZIONALE DI RIPRESA E RESILIENZA (PNRR) – MISSIONE 4 COMPONENTE 2, INVESTIMENTO 1.5); MICS (Made in Italy – Circular and Sustainable) extended partnership and received funding from the European Union Next-GenerationEU (PIANO NAZIONALE DI RIPRESA E RESILIENZA (PNRR) – MISSIONE 4 COMPONENTE 2, INVESTIMENTO 1.3 – D.D. 1551.11-10-2022, PE00000004); PRIN: Green composites based on biodegradable polymers and vegetal biomasses of Mediterranean area: processing, characterization and degradability - Bando 2022 - Prot. 20228WNZ2Z.

Data availability No datasets were generated or analysed during the current study.

Declarations

Competing interests The authors declare no competing interests.

References

1. Mohan B, Kamboj A, Virender, Singh K, Priyanka, Singh G et al (2023) Metal-organic frameworks (MOFs) materials for pesticides, heavy metals, and drugs removal: environmental safety. Sep Purif Technol 310:123175. https://doi.org/10.1016/J.SEPPUR.2023.123175
2. Jiménez-Ballesta R, Bravo S, Amorós JA, Pérez-de-los-Reyes C, García-Pradas J, Sanchez M et al (2022) Soil and Leaf Mineral element contents in Mediterranean vineyards: Bioaccumulation and potential soil Pollution. Water Air Soil Pollut 233:1–13. https://doi.org/10.1007/S11270-021-05485-6/FIGURES/2
3. Wang J, Ma T, Wei M, Lan T, Bao S, Zhao Q et al (2023) Copper in grape and wine industry: source, presence, impacts on production and human health, and removal methods. Compr Rev Food Sci Food Saf 22:1794–1816. https://doi.org/10.1111/1541-4337.13130
4. Bao Y, Reddivari L, Huang JY (2020) Development of cold plasma pretreatment for improving phenolics extractability from tomato pomace. Innovative Food Sci Emerg Technol 65:102445. https://doi.org/10.1016/J.IFSET.2020.102445
5. Dikinya O, Areola O (2010) Comparative analysis of heavy metal concentration in secondary treated wastewater irrigated soils cultivated by different crops. Int J Environ Sci Technol 7:337–346. https://doi.org/10.1007/BF03326143/METRICS
6. Gunstone T, Cornelisse T, Klein K, Dubey A, Donley N (2021) Pesticides and soil invertebrates: a Hazard Assessment. Front Environ Sci 9:643847. https://doi.org/10.3389/FENVS.2021.643847/BIBTEX
7. Alengebawy A, Abdelkhalek ST, Qureshi SR, Wang MQ (2021) Heavy metals and pesticides toxicity in agricultural soil and plants: ecological risks and human health implications. Toxics 9:42. https://doi.org/10.3390/TOXICS9030042
8. Scaffaro R, Maio A, Gammino M Electrospun polymeric nanohybrids with outstanding pollutants adsorption and electroactivity for water treatment and sensing devices. Adv Compos Hybrid Mater 2024;7. https://doi.org/10.1007/s42114-023-00827-w
9. Kapoor R, Ghosh P, Kumar M, Sengupta S, Gupta A, Kumar SS et al (2020) Valorization of agricultural waste for biogas based circular economy in India: a research outlook. Bioresour Technol 304:123036. https://doi.org/10.1016/J.BIORTECH.2020.123036
10. Rezvani Ghomi E, Khosravi F, Saedi Ardahaei A, Dai Y, Neisiany RE, Foroughi F et al (2021) The life cycle assessment for polylactic acid (PLA) to make it a low-carbon material. Polym (Basel) 13. https://doi.org/10.3390/polym13111854
11. Zhang Z, Cai S, Li Y, Wang Z, Long Y, Yu T et al High performances of plant fiber reinforced composites—A new insight from hierarchical microstructures. Compos Sci Technol 2020;194. https://doi.org/10.1016/j.compscitech.2020.108151
12. Heidari-Rarani M, Rafiee-Afarani M, Zahedi AM (2019) Mechanical characterization of FDM 3D printing of continuous carbon fiber reinforced PLA composites. Compos B Eng 175. https://doi.org/10.1016/j.compositesb.2019.107147
13. Scaffaro R, Citarrella MC, Morreale M (2023) Green Composites Based on Mater-Bi® and Solanum lycopersicum Plant Waste for 3D Printing Applications. Polymers 15:325. https://doi.org/10.3390/POLYM15020325
14. Borrero-López AM, Valencia-Barragán C, Triviño EC, Tenorio-Alfonso A, Delgado-Sánchez C, Villegas C et al (2023) Processing, characterization and disintegration properties of biopolymers based on Mater-Bi® and ellagic acid/chitosan coating. Polymers 15:1548
15. Scaffaro R, Maio A, Gulino EF, Megna B (2019) Structure-property relationship of PLA-Opuntia Ficus Indica biocomposites. Compos B Eng 167:199–206. https://doi.org/10.1016/j.compositesb.2018.12.025
16. Greco A, Gennaro R, Timo A, Bonfantini F, Maffezzoli A (2013) A comparative study between bio-composites obtained with Opuntia ficus indica Cladodes and Flax fibers. J Polym Environ 21:910–916. https://doi.org/10.1007/s10924-013-0595-x
17. Scaffaro R, Maio A, Gulino EF (2021) Hydrolytic degradation of PLA/Posidonia Oceanica green composites: a simple model based on starting morpho-chemical properties. Compos Sci Technol 213:108930. https://doi.org/10.1016/j.compscitech.2021.108930
18. Khiari R, Marrakchi Z, Belgacem MN, Mauret E, Mhenni F (2011) New lignocellulosic fibres-reinforced composite materials: a stepforward in the valorisation of the Posidonia oceanica balls. Compos Sci Technol 71:1867–1872. https://doi.org/10.1016/j.compscitech.2011.08.022
19. Scaffaro R, Lopresti F, Botta L (2018) PLA based biocomposites reinforced with Posidonia oceanica leaves. Compos B Eng 139:1–11. https://doi.org/10.1016/j.compositesb.2017.11.048
20. Gupta US, Dhamarikar M, Dharkar A, Tiwari S, Namdeo R (2020) Study on the effects of fibre volume percentage on banana-reinforced epoxy composite by finite element method.

Adv Compos Hybrid Mater 3:530–540. https://doi.org/10.1007/S42114-020-00179-9/FIGURES/15
21. Kivade SB, Gunge A, Nagamadhu M, Rajole S (2022) Mechanical and dynamic mechanical behavior of acetylation-treated plain woven banana reinforced biodegradable composites. Adv Compos Hybrid Mater 5:144–158. https://doi.org/10.1007/S42114-021-00247-8/FIGURES/20
22. Li M, Pu Y, Thomas VM, Yoo CG, Ozcan S, Deng Y et al (2020) Recent advancements of plant-based natural fiber–reinforced composites and their applications. Compos B Eng 200:108254. https://doi.org/10.1016/J.COMPOSITESB.2020.108254
23. Vedrtnam A, Kumar S, Chaturvedi S (2019) Experimental study on mechanical behavior, biodegradability, and resistance to natural weathering and ultraviolet radiation of wood-plastic composites. Compos B Eng 176. https://doi.org/10.1016/j.compositesb.2019.107282
24. Wang X, Jiang M, Zhou Z, Gou J, Hui D (2017) 3D printing of polymer matrix composites: a review and prospective. Compos B Eng 110:442–458. https://doi.org/10.1016/j.compositesb.2016.11.034
25. Rajendran Royan NR, Leong JS, Chan WN, Tan JR, Shamsuddin ZSB (2021) Current state and challenges of natural fibre-reinforced polymer composites as feeder in fdm-based 3d printing. Polym (Basel) 13. https://doi.org/10.3390/polym13142289
26. Scaffaro R, Maio A, Gulino EF, Alaimo G, Morreale M (2021) Green composites based on pla and agricultural or marine waste prepared by fdm. Polym (Basel) 13:1–17. https://doi.org/10.3390/polym13091361
27. Xu W, Jambhulkar S, Zhu Y, Ravichandran D, Kakarla M, Vernon B et al (2021) 3D printing for polymer/particle-based processing: a review. Compos B Eng 223:109102. https://doi.org/10.1016/J.COMPOSITESB.2021.109102
28. Ngo TD, Kashani A, Imbalzano G, Nguyen KTQ, Hui D (2018) Additive manufacturing (3D printing): a review of materials, methods, applications and challenges. Compos B Eng 143:172–196. https://doi.org/10.1016/J.COMPOSITESB.2018.02.012
29. Liu S, Qin S, He M, Zhou D, Qin Q, Wang H (2020) Current applications of poly(lactic acid) composites in tissue engineering and drug delivery. Compos B Eng 199:108238. https://doi.org/10.1016/J.COMPOSITESB.2020.108238
30. Scaffaro R, Citarrella MC, Gulino EF (2022) Opuntia Ficus Indica based green composites for NPK fertilizer controlled release produced by compression molding and fused deposition modeling. Compos Part Appl Sci Manuf 159:107030. https://doi.org/10.1016/J.COMPOSITESA.2022.107030
31. Fijoł N, Aguilar-Sánchez A, Ruiz-Caldas MX, Redlinger-Pohn J, Mautner A, Mathew AP (2023) 3D printed polylactic acid (PLA) filters reinforced with polysaccharide nanofibers for metal ions capture and microplastics separation from water. Chem Eng J 457:141153. https://doi.org/10.1016/J.CEJ.2022.141153
32. Gulino EF, Citarrella MC, Maio A, Scaffaro R (2022) An innovative route to prepare in situ graded crosslinked PVA graphene electrospun mats for drug release. Compos Part Appl Sci Manuf 155:106827. https://doi.org/10.1016/J.COMPOSITESA.2022.106827
33. Benito-González I, López-Rubio A, Martínez-Sanz M (2018) Potential of lignocellulosic fractions from Posidonia oceanica to improve barrier and mechanical properties of bio-based packaging materials. Int J Biol Macromol 118:542–551. https://doi.org/10.1016/j.ijbiomac.2018.06.052
34. Boudjema HL, Bendaikha H, Maschke U (2020) Green composites based on Atriplex halimus fibers and PLA matrix. J Polym Eng 40:693–702. https://doi.org/10.1515/polyeng-2020-0068
35. Tyagi P, Agate S, Velev OD, Lucia L, Pal L (2022) A critical review of the performance and soil biodegradability profiles of Biobased Natural and chemically synthesized polymers in Industrial Applications. Environ Sci Technol 56:2071–2095. https://doi.org/10.1021/ACS.EST.1C04710/ASSET/IMAGES/LARGE/ES1C04710_0009.JPEG
36. Scaffaro R, Gulino EF, Citarrella MC, Maio A (2022) Green composites based on hedysarum coronarium with outstanding FDM printability and mechanical performance. Polymers 14:1198
37. Scaffaro R, Citarrella MC, Gulino EF (2022) Morreale M Hedysarum coronarium-based Green composites prepared by Compression Molding and fused deposition modeling. Materials 15. https://doi.org/10.3390/ma15020465
38. Scaffaro R, Citarrella MC, Catania A, Settanni L (2022) Green composites based on biodegradable polymers and anchovy (Engraulis Encrasicolus) waste suitable for 3D printing applications. Compos Sci Technol 230:109768. https://doi.org/10.1016/J.COMPSCITECH.2022.109768
39. Baraldi L, De Angelis D, Bosi R, Pennini R, Bassanetti I, Benassi A et al (2022) Mechanical characterization of pharmaceutical powders by nanoindentation and correlation with their behavior during grinding. Pharmaceutics 14:1146
40. Peng Z, Jiang K, Qin Y, Li M, Balar N, O'Connor BT et al (2021) Modulation of morphological, mechanical, and Photovoltaic properties of Ternary Organic Photovoltaic blends for Optimum Operation. Adv Energy Mater 11:2003506. https://doi.org/10.1002/AENM.202003506
41. Li Y, Liang YQ, Mao XM, Li H (2022) Efficient removal of Cu(II) from an aqueous solution using a novel chitosan assisted EDTA-intercalated hydrotalcite-like compound composite: Preparation, characterization, and adsorption mechanism. Chem Eng J 438. https://doi.org/10.1016/j.cej.2022.135531
42. Cremonezzi JM, de O, Pinto GM, Mincheva R, Andrade RJE, Raquez JM, Fechine GJM (2023) The micromechanics of graphene oxide and molybdenum disulfide in thermoplastic nanocomposites and the impact to the polymer-filler interphase. Compos Sci Technol 243. https://doi.org/10.1016/j.compscitech.2023.110236
43. Baek K, Shin H, Cho M Multiscale modeling of mechanical behaviors of Nano-SiC/epoxy nanocomposites with modified interphase model: Effect of nanoparticle clustering. Compos Sci Technol 2021;203. https://doi.org/10.1016/j.compscitech.2020.108572
44. Tao Y, Liu M, Han W, Li P (2021) Waste office paper filled polylactic acid composite filaments for 3D printing. Compos B Eng 221:108998. https://doi.org/10.1016/J.COMPOSITESB.2021.108998
45. Liu Z, Lei Q, Xing S (2019) Mechanical characteristics of wood, ceramic, metal and carbon fiber-based PLA composites fabricated by FDM. J Mater Res Technol 8:3743–3753. https://doi.org/10.1016/j.jmrt.2019.06.034
46. Kiendl J, Gao C (2020) Controlling toughness and strength of FDM 3D-printed PLA components through the raster layup. Compos B Eng 180:107562. https://doi.org/10.1016/J.COMPOSITESB.2019.107562
47. Andrzejewski J, Cheng J, Anstey A, Mohanty AK, Misra M (2020) Development of toughened blends of poly(lactic acid) and poly(butylene adipate- co-terephthalate) for 3D Printing Applications: compatibilization methods and material performance evaluation. ACS Sustain Chem Eng 8:6576–6589. https://doi.org/10.1021/ACSSUSCHEMENG.9B04925/ASSET/IMAGES/LARGE/SC9B04925_0008.JPEG
48. Tang Y, Varyambath A, Ding Y, Chen B, Huang X, Zhang Y et al (2022) Porous organic polymers for drug delivery: hierarchical pore structures, variable morphologies, and biological properties. Biomater Sci 10:5369–5390. https://doi.org/10.1039/D2BM00719C
49. Scaffaro R, Gulino EF, Citarrella MC (2023) Biodegradable membrane with high porosity and Hollow structure obtained via Electrospinning for oil spill clean-up application. J Polym Environ 31:3965–3981. https://doi.org/10.1007/s10924-023-02876-0
50. Souza JdeL, Chiaregato CG, Faez R (2018) Green Composite based on PHB and Montmorillonite for KNO3 and NPK Delivery

System. J Polym Environ 26:670–679. https://doi.org/10.1007/s10924-017-0979-4
51. El Gharrak A, Essamlali Y, Amadine O, Aboulhrouz S, Hafnaoui A, Ghalfi H et al (2022) Tunable physicochemical properties of lignin and rapeseed oil-based polyurethane coatings with tailored release property of coated NPK fertilizer. Prog Org Coat 170:106982. https://doi.org/10.1016/J.PORGCOAT.2022.106982
52. Ramírez-Rodríguez GB, Dal Sasso G, Carmona FJ, Miguel-Rojas C, Pérez-De-Luque A, Masciocchi N et al (2020) Engineering Biomimetic Calcium phosphate nanoparticles: a Green synthesis of slow-release multinutrient (NPK) Nanofertilizers. ACS Appl Bio Mater 3:1344–1353. https://doi.org/10.1021/ACSABM.9B00937/ASSET
53. Das SK, Ghosh GK (2021) Developing biochar-based slow-release N-P-K fertilizer for controlled nutrient release and its impact on soil health and yield. Biomass Convers Biorefin 1:1–13. https://doi.org/10.1007/S13399-021-02069-6/TABLES/5
54. Ritger PL, Peppas NA (1987) A simple equation for description of solute release II. Fickian and anomalous release from swellable devices. J Controlled Release 5:37–42. https://doi.org/10.1016/0168-3659(87)90035-6
55. Wu IY, Bala S, Škalko-Basnet N, di Cagno MP (2019) Interpreting non-linear drug diffusion data: utilizing Korsmeyer-Peppas model to study drug release from liposomes. Eur J Pharm Sci 138:105026. https://doi.org/10.1016/j.ejps.2019.105026
56. Chen YC, Chen YH (2019) Thermo and pH-responsive methylcellulose and hydroxypropyl hydrogels containing K2SO4 for water retention and a controlled-release water-soluble fertilizer. Sci Total Environ 655:958–967. https://doi.org/10.1016/j.scitotenv.2018.11.264
57. Torres FG, Dioses-Salinas DC, Pizarro-Ortega CI, De-la-Torre GE (2021) Sorption of chemical contaminants on degradable and non-degradable microplastics: recent progress and research trends. Sci Total Environ 757:143875. https://doi.org/10.1016/J.SCITOTENV.2020.143875
58. Zhou T, Zhao M, Zhao X, Guo Y, Zhao Y (2021) Simultaneous remediation and fertility improvement of heavy metals contaminated soil by a novel composite hydrogel synthesized from food waste. Chemosphere 275:129984. https://doi.org/10.1016/J.CHEMOSPHERE.2021.129984